Proceedings of the Sixth International Conference on
Railway Technology: Research, Development and Maintenance
Edited by: J. Pombo
Civil-Comp Conferences, Volume 7, Paper 4.3
Civil-Comp Press, Edinburgh, United Kingdom, 2024
ISSN: 2753-3239, doi: 10.4203/ccc.7.4.3

The Relevance of Non-Linear Dynamics on Railway Pantographs

J. Gil Romero, S. Gregori, M. Tur and F. J. Fuenmayor

**Institute of Mechanical Engineering and Biomechanics,
Universitat Politecnica de Valencia, Spain**

Abstract

The pantograph-catenary dynamic interaction is widely studied by computational simulations, which depend on accurate models to provide faithful results. In this paper, we particularly deal with the modelling of the DSA-380 pantograph. Firstly, experimental tests are conducted to evaluate the dynamic behaviour of the pantograph and the importance of the non-linearities in it. The non-linear behaviour is evidenced if a frequency response function changes when the excitation applied changes. In this work, we identify the nature of the non-linearities and the specific parts where they come from. Then, we create a model able to emulate the dynamics of the real pantograph with a simple but effective design. The model is a lumped mass model with a non-linear system for the pantograph head suspension, which includes geometric non-linearities and dry friction. The model is able to reproduce successfully the frequency response functions of the pantograph even though it is an uncomplicated model in which only the necessary elements are included. Besides the development of the model, this work also proposes an efficient strategy to integrate the dynamic equation with Coulomb friction, showing good performance even with slip/stick transitions.

Keywords: pantograph, non-linear, modelling, experimental test, frequency response analysis, pantograph-catenary interaction.

1 Introduction

The pantograph-catenary interaction is widely studied by computational simulations as demonstrated by the large collection of works that the benchmark exercise [2] includes. The accuracy of simulations relies on the formulation of the models, the fidelity of the topology, material properties and, in general, the similitude of every modelled part with the real system. Some of those parts are simplified in the model; others are defined using measurements, experimental adjustment or other techniques that allow efficient modelling of the whole system and fidelity regarding the tangible arrangement. In fact, the simulations can be validated according to the European Standard EN 50318 [3], which ensures the reliability of the results.

The pantograph model is responsible for a big portion of the simulation accuracy and developing accurate pantograph models is a challenge. This is due to the high number of pieces and the uncertainty of the dynamic behaviour of some parts that are hard to model. For example, the presence of clearances, dry friction, non-linear contact, etc. makes it very hard to describe a model that reproduces the dynamic behaviour of the pantograph in a wide range of operating conditions.

The pantograph models featured in research works predominantly comprise lumped mass models, as exemplified by [10], which effectively replicate the foundational aspects of pantograph linear dynamics within the 20 Hz frequency range. For the representation of higher frequency components, it becomes imperative to account for the elasticity in pantograph contact strips. This consideration is notably addressed in the multi-mass system proposed by [7], which also incorporates the wear profile of the contact strip. Furthermore, in the work of [8], the non-linear characteristics of the pantograph damper are considered, emphasizing its significance within a rigid multi-body pantograph framework. Another notable category of pantograph models is the flexible multi-body, as the model developed in [1], which is an upgrade with respect to rigid multi-body systems.

The accuracy of pantograph models is contingent upon effective parameter identification. In this matter, [9] adopts a disassembly and testing approach, wherein different components of the pantograph are subjected to individual tests to calibrate inertia and dissipative parameters. After this process, a final evaluation of the assembled pantograph is conducted with a unit-step load test. However, parameter identification is commonly carried out in the literature by fitting dynamic measurements of the whole pantograph.

Other features can be incorporated in the pantograph models, such as the non-ideal joint that allows relative displacement considered in [11] within a flexible multi-body pantograph. Additionally, external aerodynamic forces constitute another facet of pantograph modelling, as shown in [5]. This work provides a detailed guide to incorporate aerodynamic forces and assesses their influence on the contact force.

The present work deals with the analysis of pantograph non-linear behaviour: how much non-linear models are necessary and how to develop those models. The im-

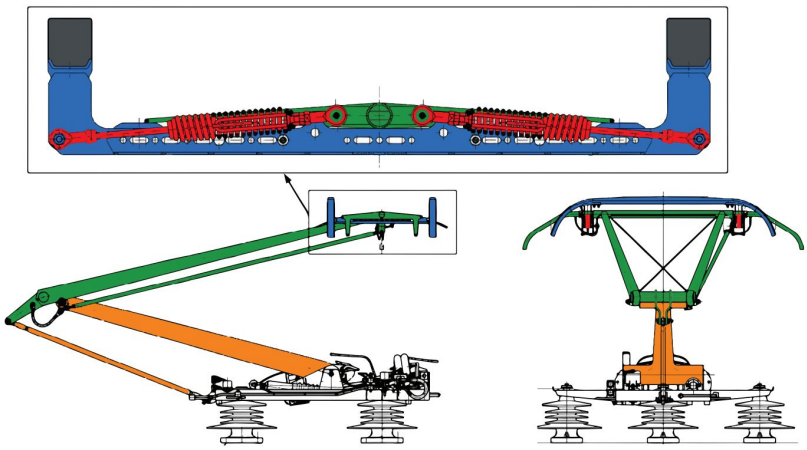

Figure 1: DSA 380 pantograph.

portance of the non-linearities in the pantograph dynamics depends on every specific model and it can be assessed by experimental pantograph tests. Also, different sources of non-linearity (friction, geometric, contact, etc.) can be present in the different pantographs and there is no general rule to find the right kind of non-linear model for every case. Thus, here we study the pantograph DSA-380. Firstly, we collect the experimental measurements that evidence the pantograph non-linear behaviour; then, we find the part of the pantograph where that behaviour originates and develop a simple non-linear model that explains it.

2 Experimental analysis of the pantograph

DSA-380 is a model of pantograph employed in high-speed trains, which has the arrangement shown in Fig. 1, where the main parts of the pantograph are distinguished in different colours. The pantograph head is marked in blue, which has two contact strips and is suspended with four oblique springs (marked in red). Those springs are connected with the upper frame (marked in green), which in turn is joined with the lower frame (marked in orange).

One of the most used techniques to describe the dynamic of the pantograph is the use of Frequency Response Functions (FRF). Particularly, it is fairly common to use the spectral ratio between the pantograph head vertical displacement and a vertical force applied at the centre of the pantograph head. This kind of analysis is intended for models with linear behaviour since they have unique FRFs. On the contrary, this does not happen with non-linear systems since there is not an independent relation between the different frequencies of the spectrum. However, it is possible to apply non-linear Frequency Response Analysis (NFRA) to analyse non-linear systems and quantify the level of non-linearity. In this case, a first-order frequency response function $H_1(\omega)$ at frequency ω is defined as the spectral ratio of the response to the excitation force when the excitation is a harmonic function of frequency ω and all the other

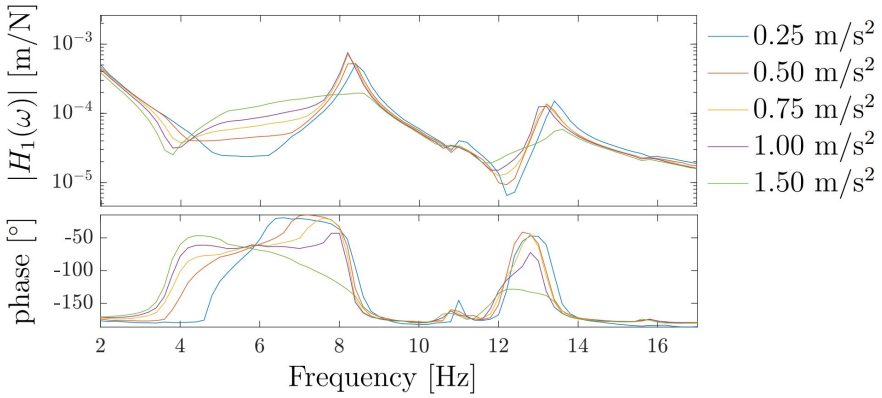

Figure 2: First-order FRF measurements of the DSA-380 for different excitation amplitudes.

harmonic components are not considered. Since the first-order FRF depends on the amplitude of the excitation and any other features of it, the particular excitation technique used should be determined and it is linked to the results. Here, pure (as far as the control system allows it) sinusoidal displacement signals are repeatedly imposed, varying the frequency to obtain the first-order FRF $H_1(\omega)$ by computing every time the force-frequency content at ω. The several FRFs obtained in the test bench for different amplitudes are shown in Fig. 2. The grade of non-linearity is evidenced by the difference between the curves and it is more abrupt in some domains of the spectrum.

3 Pantograph model

After observing, in the previous section, the dynamic behaviour of the pantograph we want to model, the objective is to find a model able to reproduce that. The strategy we follow is to start by finding a linear model to evaluate how well or badly it works and then we will try to find which are the non-linear features that are lacking to explain/reproduce the experimental data.

3.1 Linear model

The conventional lumped mass model shown in Fig. 3 (a) is a well-established model for pantograph modelling. Note that the colours employed in the figure are those of Fig. 1 in order to relate the parts of the model with the parts of the pantograph. Note also that the stiffness k_1^{eq} represents the four oblique springs of the real pantograph.

This model has a FRF relating the displacement of the upper mass to the force applied at the same point and the FRF is the same no matter how the excitation is or if it is computed as a conventional or a first-order FRF. Thus, the linear model cannot imitate the behaviour that we found in Fig. 2 with multiple curves. However, we can try to tune the parameters of the model in order to fit the experimental curve

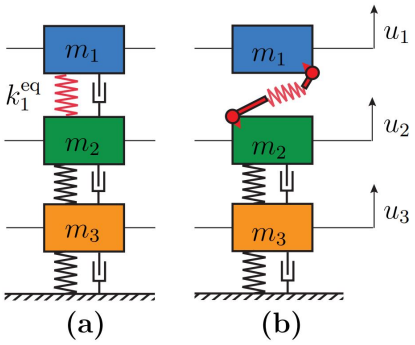

Figure 3: (a) Three degree of freedom linear model and (b) three degree of freedom model with Z-spring.

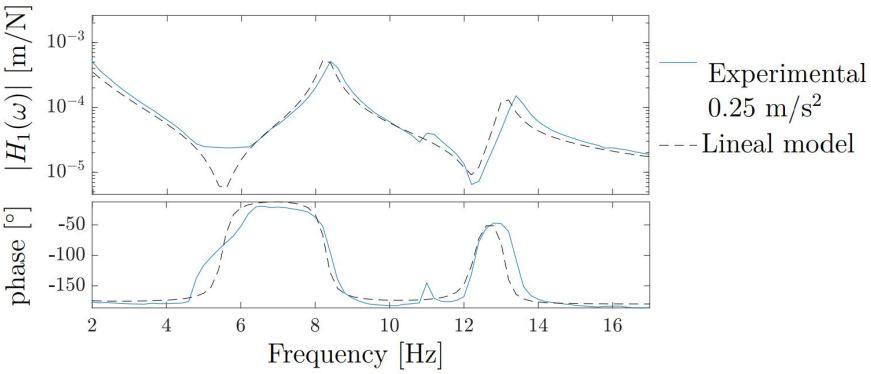

Figure 4: First-order FRF measurements of the DSA-380 for excitation of 0.25 m/s^2 and the adjusted lineal model.

with the smallest amplitude (0.25 m/s^2) since smaller amplitudes exhibit a more linear behaviour. In Fig. 4 the result of this fitting is shown in which the linear model is optimised to reduce the mean square error between both curves. The agreement between both curves is acceptable but the model is not robust because it is only valid for small amplitude and pure harmonic excitation.

3.2 Non linear model

After getting a linear model that fairly fits the dynamic behaviour of the pantograph for small amplitudes and observing the non-linear behaviour in Fig. 2, the questions that arise are: what model will be able to show a similar response as the observed in tests and what lacks the linear model. Looking at the pantograph in Fig. 1, it is obvious that the linear model is a vast simplification or more accurately a cluster of simplifications: not considering geometric non-linearities of oblique bars, non including a non-linear damper, lacking dry friction, not considering the flexibility of the bars, non-including more degrees of freedom, etc. However, addressing all the simplifications is not the most efficient way of solving the problem and it does not ensure that the model is

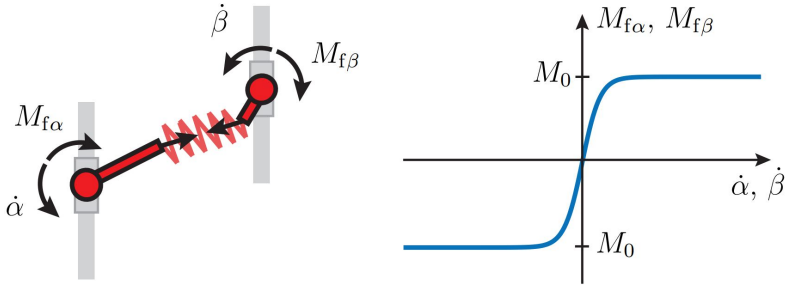

Figure 5: Z-spring configuration and friction at the two joints.

(a) (b)

Figure 6: Z-spring movement when (a) friction block the bars and (b) friction is negligible.

going to be accurate.

We have found that the oblique springs of the pantograph head suspension, shown in red in Fig. 1 can be responsible for most part of the non-linearities measured in the tests. The suspicion comes from the fact that we have measured statically the equivalent stiffness of the pantograph head suspension and the value differs significantly (approximately half) from the equivalent stiffness k_1^{eq} of the linear model, which was obtained by means of dynamic measurements. This fact cannot be explained by a simple oblique pre-stressed spring; thus, a more thorough modelling is necessary. As it can be seen in Fig. 1, every of the pantograph head springs is made up of three pieces: there is a spring and two rods that connect it with the other parts of the pantograph by revolution joints. This configuration can be modelled as seen in Fig. 5 also including dry friction in the joints; it is going to be called Z-spring since its three parts arrangement. Fortunately, this model can explain the different values found for the equivalent stiffness k_1^{eq}. When this stiffness is obtained by fitting the small-amplitude FRF, a bigger value is found because, in that case, the friction forces are enough to constrain the rotation of the rods and the Z-spring moves as shown in Fig. 6 (a). However, when the stiffness is measured in a static test where the amplitude employed is much bigger the friction forces are negligible and the Z-spring moves as in Fig. 6 (b), resulting in a smaller equivalent stiffness.

Since the Z-spring non-linear system is seemingly important for the pantograph dynamics and a linear spring could not be a good representation of the pantograph head suspension, the Z-spring is going to be featured in the non-linear pantograph model as can be seen in Fig. 3 (b). Note that this element is replacing four of the pantograph oblique springs because we assume here that the movements of all of

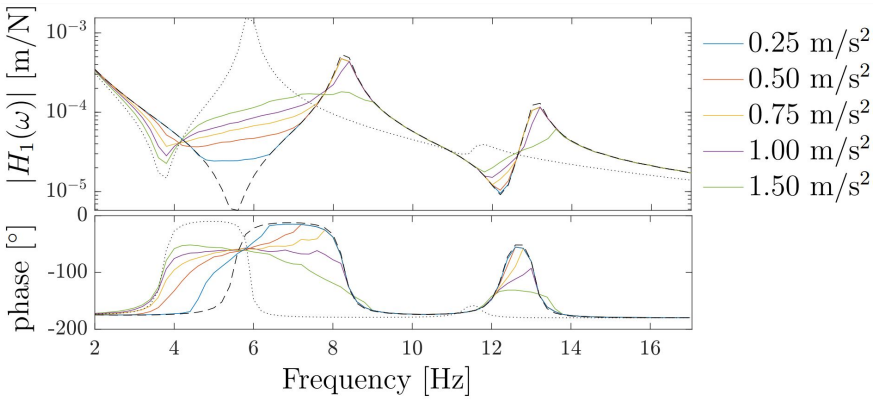

Figure 7: First-order FRF obtained by simulations of the three degrees of freedom with Z-spring model (coloured lines), linear model 1 (dashed line) and linear model 2 (dotted line) for different excitation amplitudes.

them are the same. Note also that the model has gone from the three d.o.f. of the linear model to the 5 d.o.f of this one that includes the angles α and β of the two rods (see Fig. 5).

With the inclusion of the Z-spring, some extra parameters have to be defined in the model. The lengths of the bars can be measured but the stiffness and undeformed length of the spring and the maximum friction moment at the joints M_0 have to be adjusted without disassembling the pieces. Those parameters can be optimised to reduce the mean square error with respect to the experimental data.

The non-linear model can be simulated following the method explained in Section 4 to compute the first-order FRF using harmonic displacement excitation with different amplitudes. The results are shown in Fig. 7 where similar curves to the experimental ones (Fig. 2) are observed. This fact implies that the non-liar behaviour is mainly explained by the Z-spring system and other simplifications adopted in the model are not as important as the linearization of the pantograph head suspension.

The behaviour of this model is non-linear and complex, but it is possible to provide an understanding of its dynamic with two linear models. Those are obtained by linearising the non-linear model using two different hypotheses. The first linear model assumes that the friction is enough to constrain the rotation of the revolution joints so the rods of the Z-spring are fixed as in Fig. 6 (a). The second linear model assumes that the friction is zero and the movement corresponds with the one shown in 6 (b). In Fig. 7, the FRF of those two models are plotted with the dashed and dotted black lines respectively. The movement of the non-linear model seems to be bounded by the two linear models and there are zones where the non-linear model is very similar to one of the linear models because the corresponding hypothesis is true.

4 Numerical methods

This Section is devoted to explaining the mathematical procedures carried out in the previous sections to simulate the pantograph model. The first step is to gather the degrees of freedom of the non-linear model (Fig. 3) in a vector:

$$\mathbf{u} = [u_1 \quad \alpha \quad \beta \quad u_2 \quad u_3]^\top \tag{1}$$

those are governed by the equation:

$$\mathbf{M}\ddot{\mathbf{u}} + \mathbf{C}\dot{\mathbf{u}} + \mathbf{F}^{\mathrm{e}}(\mathbf{u}) + \mathbf{F}^{\mathrm{f}}(\dot{\mathbf{u}}) = \mathbf{F} \tag{2}$$

where $\mathbf{M}$, $\mathbf{C}$ are the mass matrix and damping matrix, $\mathbf{F}^{\mathrm{e}}$ is the elastic generalised forces in degrees of freedom, $\mathbf{F}^{\mathrm{f}}$ is Coulomb friction generalised forces and $\mathbf{F}$ the external forces. The elastic forces coming from the Z-spring have a non-linear formulation whereas the others coming from the linear springs can be written linearly, thus, the elastic forces can be expressed as:

$$\mathbf{F}^{\mathrm{e}} = \mathbf{F}^{\mathrm{eNL}} + \mathbf{K}^{\mathrm{L}}\mathbf{u} \tag{3}$$

where $\mathbf{F}^{\mathrm{eNL}}$ is the non-linear elastic forces and $\mathbf{K}^{\mathrm{L}}$ is the stiffness matrix that only considers the linear springs of the model.

The Z-spring is formed by two rigid rods of lengths L_1 y L_2 and a spring of stiffness k. This element elastic forces are derived by differentiating potential energy with respect to the d.o.f. in compliance with the Euler-Lagrange equation. :

$$E_{\mathrm{p}} = \frac{1}{2}k(l - l_0)^2 \tag{4}$$

where the length l is:

$$\begin{array}{l} l = \sqrt{(L_1\mathrm{C}_\alpha + L_2\mathrm{C}_\beta - d)^2 + (-L_1\mathrm{S}_\alpha - L_2\mathrm{S}_\beta + u_2 - u_1)^2} \\ \mathrm{C}_\alpha = \cos\alpha;\ \mathrm{S}_\alpha = \sin\alpha;\ \mathrm{C}_\beta = \cos\beta;\ \mathrm{S}_\beta = \sin\beta \end{array} \tag{5}$$

where d is the horizontal distance between the two joints. Deriving the potential energy we find:

$$\mathbf{F}^{\mathrm{eNL}} = \frac{2k_1(l - l_0)}{l} \begin{bmatrix} u_1 - u_2 + L_2\mathrm{S}_\beta + L_1\mathrm{S}_\alpha \\ L_2\mathrm{C}_\beta(u_1 - u_2 + L_2\mathrm{S}_\beta + L_1\mathrm{S}_\alpha) - L_2\mathrm{S}_\beta(L_2\mathrm{C}_\beta - d + L_1\mathrm{C}_\alpha) \\ L_1\mathrm{C}_\alpha(u_1 - u_2 + L_2\mathrm{S}_\beta + L_1\mathrm{S}_\alpha) - L_1\mathrm{S}_\alpha(L_2\mathrm{C}_\beta - d + L_1\mathrm{C}_\alpha) \\ -(u_1 - u_2 + L_2\mathrm{S}_\beta + L_1\mathrm{S}_\alpha) \\ 0 \end{bmatrix} \tag{6}$$

The Coulomb friction at the two revolution joints of the Z-spring (see Fig. 5) is dependent on the velocity of the d.o.f. The maximum friction allowed is M_0 and the

hyperbolic tangent function regularises the Coulomb law:

$$\mathbf{F}^{\mathrm{f}} = M_0 \begin{bmatrix} 0 \\ \tanh \tau \dot{\alpha} \\ \tanh \tau \dot{\beta} \\ 0 \\ 0 \end{bmatrix} \tag{7}$$

where τ determines how soft the function is, the higher τ is the higher the accuracy, but it exhibits lesser numerical stability. A value of $\tau = 1000$ s has been chosen since bigger values do not improve accuracy significantly.

Finally, the mass $\mathbf{M}$, damping $\mathbf{C}$ and stiffness $\mathbf{K}^{\mathrm{L}}$ matrices are obtained by assembling by including the masses, linear dampers and linear springs of the model.

Once all the terms of Eq. (2) are totally defined, it can be solved by carrying out an integration scheme algorithm. This problem implies certain difficulties since the Coulomb friction provokes unceasing shifts between slip and stick state. A strategy to solve this kind of problem is presented in [6], in which a specific regularization of the Coulomb law and the 4^{th} order Runge-Kutta scheme is employed. However, after applying that method in this case, we found that the method requires too small time increment so the computational cost was high. Thus we have choose to use the HHT (Hilber-Hughes-Taylor) implicit integration scheme [4] and the Newton-Raphson method to solve the implicit equation every time step. However, the Newton-Raphson method has convergence issues when applied to this problem; frequently the iterative solution jumps between two states S_1 and S_2 as shown in Fig. 8. This problem is solved if the tangent matrix is modified by altering the derivative of the $\tanh$ that appears in friction law. Originally the derivative of $\tanh$ is:

$$g_1(\dot{\alpha}) = \frac{\mathrm{d} \tanh \dot{\alpha}}{\mathrm{d}\dot{\alpha}} = \mathrm{sech}^2 \dot{\alpha} \tag{8}$$

the proposed fake derivative $g_2(\dot{\alpha})$ is the slope of the line defined by the origin and the point where the derivative is evaluated (see Fig. 8):

$$g_2(\dot{\alpha}) = \frac{\tanh \dot{\alpha}}{\dot{\alpha}} \tag{9}$$

Changing g_1 by g_2, the convergence issues does not longer appear and using $g = 0.5(g_1 + g_2)$ reduces the number of iterations.

This approach has demonstrated significantly less computationl cost compared to the fourth-order Runge-Kutta method, primarily due to its capacity to accommodate substantially larger time steps while maintaining equivalent accuracy levels. As a general guideline, the suggested technique achieves comparable accuracy to the ODE45 function in Matlab® , utilising a time increment 2000 times larger and requiring 250 times less computation time. For the results of this work, we use a 2 ms time step and a numerical damping of $\alpha = -0.3$

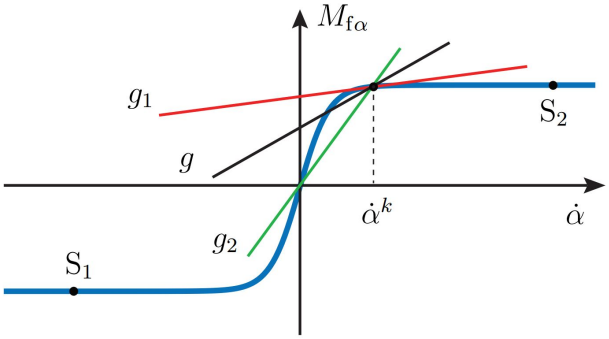

Figure 8: Regularisation of Coulomb law and modified derivative for improving convergence of Newton-Raphson method.

5 Conclusions and contributions

In this paper, a specific pantograph is studied in order to develop a model that reproduces its dynamic behaviour. Experimental tests of the pantograph are performed and the frequency analysis allows recognising the presence of non-linearities in the pantograph. Therefore, the pantograph model has to be able to exhibit non-linear features like the one found in the tests. We have designed a pantograph model, considering only the essential features, which provides a good agreement with the measurements while also giving a clear understanding of its non-linear dynamics. The challenge of this work is to find the non-linear model that fits well the dynamic of the pantograph since there is no general rule to model non-linear systems and the pantograph is a complex mechanism with a lot of pieces of different kinds. The key element that has added the non-linear feature to the model is a Z-spring, which is a linkage of three pieces with dry friction. The final conclusion is that linear models can be insufficient, and non-linearities are relevant in pantograph dynamics. An additional contribution of this work is the proposition of an efficient integration scheme to integrate the system, reducing computational cost.

Acknowledgements

This work is possible due to the support received from the State Research Agency of the Spanish Science and Innovation Ministry (PID2020-113458RB-I00) and from the Valencian Regional Government (PROMETEO/2021/046).

References

[1] Jorge Ambrósio, Frederico Rauter, Joao Pombo, and Manuel S Pereira. A flexible multibody pantograph model for the analysis of the catenary–pantograph contact. *Multibody dynamics: computational methods and applications*, pages 1–27, 2011.

[2] Stefano Bruni, Jorge Ambrosio, Alberto Carnicero, Yong Hyeon Cho, Lars Finner, Mitsuru Ikeda, Sam Young Kwon, Jean Pierre Massat, Sebastian Stichel, and Manuel Tur. The results of the pantograph-catenary interaction benchmark. *Vehicle System Dynamics*, 53(3):412–435, 2015.

[3] EN 50318:2018. Railway applications. Current collection systems. Validation of simulation of the dynamic interaction between pantograph and overhead contact line. *European Union Agency for Railways*, 2018.

[4] Hans M Hilber, Thomas J R Hughes, and Robert L Taylor. Improved numerical dissipation for time integration algorithms in structural dynamics. *Earthquake Engineering & Structural Dynamics*, 5(3):283–292, 1977.

[5] J. Pombo, J. Ambrósio, M. Pereira, F. Rauter, A. Collina, and A. Facchinetti. Influence of the aerodynamic forces on the pantograph–catenary system for high-speed trains. *Vehicle System Dynamics*, 47(11):1327–1347, 2009.

[6] D. Dane Quinn. A New Regularization of Coulomb Friction . *Journal of Vibration and Acoustics*, 126(3):391–397, 07 2004.

[7] Dongli Song, Yanan Jiang, and Weihua Zhang. Dynamic performance of a pantograph–catenary system with consideration of the contact surface. *Proceedings of the Institution of Mechanical Engineers, Part F: Journal of Rail and Rapid Transit*, 232(1):262–274, 2018.

[8] Wenlin Wang, Yuwen Liang, and Weihua Zhangand Simon Iwnicki. Effect of the nonlinear displacement-dependent characteristics of a hydraulic damper on high-speed rail pantograph dynamics. *Nonlinear Dynamics*, 95(4):3439–3464, 2019.

[9] Andrzej Wilk, Len Gelman, Slawomir Judek, Krzysztof Karwowski, Mirosław Mizan, Tadeusz Maciołek, Miroslaw Lewandowski, Aleksander Jakubowski, and Karolina Klimowska. Novel method of estimation of inertial and dissipative parameters of a railway pantograph model. *Vehicle System Dynamics*, 60(7):2413–2435, 2022.

[10] Ning Zhou and Weihua Zhang. Investigation on dynamic performance and parameter optimization design of pantograph and catenary system. *Finite Elements in Analysis and Design*, 47(3):288–295, 2011.

[11] Ming Zhu, Sara Ying Zhang, Jason Zheng Jiang, John Macdonald, Simon Neild, Pedro Antunes, Joâo Pombo, Stephen Cullingford, Matthew Askill, and Stephen Fielder. Enhancing pantograph-catenary dynamic performance using an inertance-integrated damping system. *Vehicle System Dynamics*, 60(6):1909–1932, 2022.